Electronic coherence and coherent dephasing in the optical control of electrons in graphene

Christian Heide,[1,*] Timo Eckstein,[1,*] Tobias Boolakee,[1] Constanze Gerner,[1] Heiko B. Weber,[2] Ignacio Franco,[3] and Peter Hommelhoff[1]

[1]*Laser Physics, Department of Physics, Friedrich-Alexander-Universität Erlangen-Nürnberg (FAU), Staudtstrasse 1, D-91058 Erlangen, Germany*
[2]*Applied Physics, Department of Physics, Friedrich-Alexander-Universität Erlangen-Nürnberg (FAU), Staudtstrasse 7, D-91058 Erlangen, Germany*
[3]*Departments of Chemistry and Physics, University of Rochester, Rochester, New York 14627, USA*
(Dated: July 15, 2021)

Electronic coherence is of utmost importance for the access and control of quantum-mechanical solid-state properties. Using a purely electronic observable, the photocurrent, we measure an electronic coherence time of 22 ± 4 fs in graphene. The photocurrent is ideally suited to measure electronic coherence as it is a direct result of quantum path interference, controlled by the delay between two ultrashort two-color laser pulses. The maximum delay for which interference between the population amplitude injected by the first pulse interferes with that generated by the second pulse determines the electronic coherence time. In particular, numerical simulations reveal that the experimental data yield a lower boundary on the electronic coherence time and that coherent dephasing masks a lower coherence time. We expect that our results will significantly advance the understanding of coherent quantum-control in solid-state systems ranging from excitation with weak fields to strongly driven systems.

Within the last 25 years, the role of electronic coherence is pivotal in ultrafast optoelectronics [1–6]. Several experimental schemes has been applied to study the underlying lifetime of coherence, which can range from picoseconds in cold atoms [7, 8] down to the sub-femtosecond timescales in highly excited semiconductors and metals [1, 9, 10]. One key to measure coherence is the access to an interference process, such as used in coherent spectroscopy [4, 9, 11] or four-wave mixing [12]. As a counterpart to these experiments relying on optical polarization, we will show that a current, which is a direct result of quantum interference in solids, can serve as ideal observable to measure electronic coherence in solids. While there are various measurements demonstrating the coherent control in solids [13–18], the underlying timescale of electronic coherence is mostly obscured due to the lack of ultrafast pulses.

In particular, light of low temporal symmetry can generate net currents in solids, even in the absence of a bias voltage or spatial asymmetries in the material [5, 13–15, 17, 19–21]. In the perturbative limit, such light-induced symmetry breaking arises due to the interference of an even and odd order pathway from a given initial to a final momentum state, as schematically shown in Fig. 1a for one- versus two-photon absorption [13–16, 22, 23]. By changing the relative phase between the two colors, the quantum interference and, thus, the net current amplitude and direction can be controlled. Intriguingly, this interference process persists beyond the perturbative regime and expands to the strong-field regime. In this case, the interference between intra- and interband light-induced electron dynamics leads to a phase-controllable
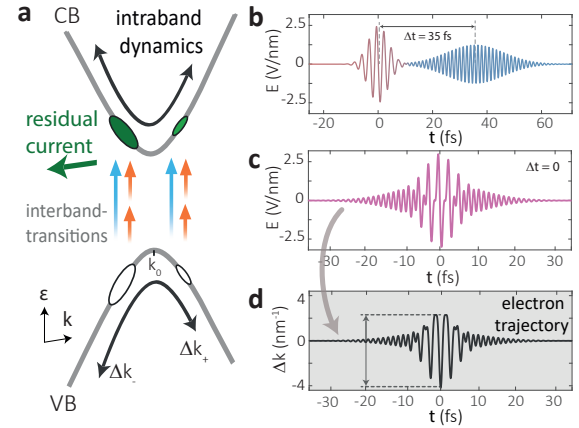
FIG. 1. **Electron control using $\omega + 2\omega$ two-color laser fields. a**, Schematic illustration of two-color quantum path interference near the band gap. The interference of one- vs. two-photon excitation generates a phase-dependent asymmetry in the electron/hole population distribution, giving rise to a residual current. **b, c**, Electric field waveform of a 6 fs few-cycle laser pulse and its second harmonic with a pulse duration of 19 fs for a temporal delay of $\Delta t = 35$ fs (**b**) and $\Delta t = 0$ (**c**). **d**, The light-induced electron dynamics exhibit a clear negative peak in momentum space (k-space), breaking the inversion symmetry of graphene (black arrows in (**a**)). The trajectory is obtained from the Bloch acceleration theorem: $\dot{k}(t) = -\hbar^{-1}eE(t)e$.

current [5, 24–26]. In all these regimes, the current requires electronic coherence to emerge as it relies on interference [27]. Scattering with other electrons or phonons are sources of decoherence, leading to a suppression of the light-injected current, as the electrons loose its ability to interfere [1, 9, 28, 29]. Whereas the current is a purely electronic observable arising from electron interference,

* These two authors contributed equally

commonly applied methods to measure coherence, based on the optical response of matter, rely on measuring the optical polarization. While such measurements offer information about coherence between optically active states it is often hard to disentangle electronic and vibrational contributions to the resulting signal, making it challenging to directly measure electronic coherence [9, 30–32].

In this Letter, we demonstrate the ability to monitor electronic coherence by injecting a two-color induced photocurrent in graphene. The combined two-color optical field is described as $E(t) = E_\omega(t) \cdot \cos(\omega t + \varphi_\omega) + E_{2\omega}(t + \Delta t) \cdot \cos(2\omega(t + \Delta t) + \varphi_{2\omega})$, with Δt the delay between both pulses, and $E_\omega(t)$ and $E_{2\omega}(t + \Delta t)$ are the envelope functions of the laser pulses with angular frequencies of ω and 2ω. To lowest order, the current density j emerges as a third order process in the photoresponse [13–15, 21, 27]:

$$j \propto E_{0,2\omega} E_{0,\omega}^2 \sin(2\varphi_\omega - \varphi_{2\omega} - 2\omega\Delta t), \qquad (1)$$

where $E_{0,\omega}$ and $E_{0,2\omega}$ are the peak field strengths. The dependence of the relative phase on the time delay between the two colors is given by $\varphi_{\text{Delay}}(\Delta t, \omega) = 2\omega\Delta t$ [13, 14, 23].

The formalism that leads to Eq.(1) requires continuous wave excitation, where only excitation separated by $2\hbar\omega$ contributes to the net current (see blue and red arrows in Fig. 1a). When short and strong laser pulses are applied to a continuum of resonant states, intraband motion may become important and deviations from Eq. (1) can occur, which we will discuss later based on numerical simulations.

In the experiment, we focus two laser fields to the center of a $10 \times 2\,\mu m^2$ graphene strip, a few-cycle fundamental and a frequency-doubled femtosecond laser field. The monolayer graphene is epitaxially grown on silicon carbide (4H-SiC) and connected to two electrodes [5]. The laser beam radii are $1.9 \pm 0.1\,\mu m$ ($1/e^2$ intensity) for both the ω and 2ω beams and, thus, the electrodes are hardly illuminated by the laser field. The sample is placed in vacuum ($\approx 10^{-6}$ hPa). Laser pulses from an 80-MHz-Ti:Sapphire laser oscillator with a center wavelength of 800 nm are frequency doubled using a beta barium borate (BBO) crystal. Both colors are separately controlled in a two-color interferometer and sent to the sample. This setup allows independent control of relative phase, intensity, polarization, and dispersion. The resulting pulse duration of $\tau_\omega = 6.0 \pm 0.5$ fs (intensity full width at half maximum (FWHM)) for the fundamental is measured via spectral phase interferometry for direct electric-field reconstruction (SPIDER), while its second harmonic with a pulse duration of $\tau_{2\omega} = 19 \pm 2$ fs (17 fs Fourier limit) is determined via a cross-correlation frequency-resolved optical gating (XFROG). We note that both pulses do not spectrally overlap and, thus, optical interference between both pulses does not occur. We perform a lock-in measurement referenced to a periodic modulation of the temporal delay between both colors to isolate the rela-
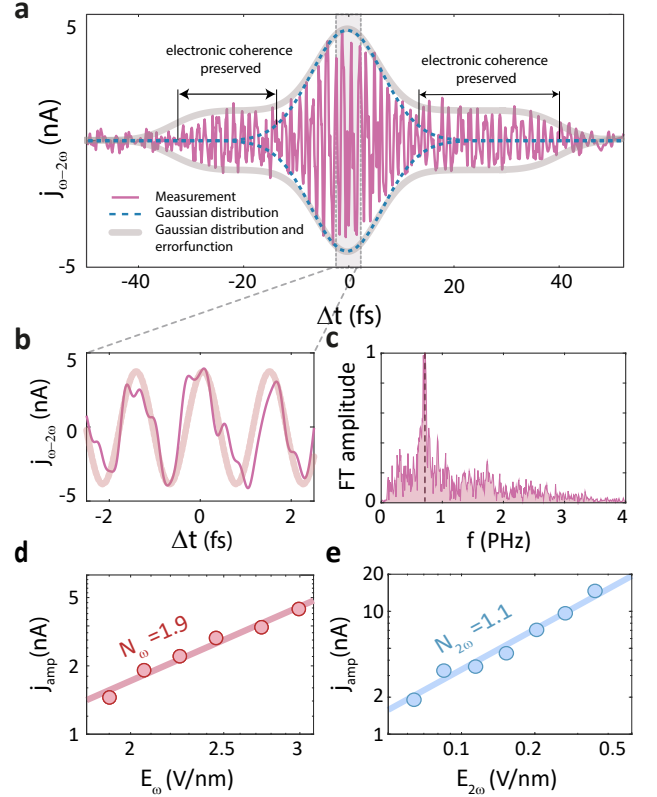
FIG. 2. **Coherent $\omega + 2\omega$ phase-controlled current generation in graphene. a**, Measured current as a function of temporal delay Δt. $\Delta t < 0$ means that the 2ω-pulse arrives before the ω-pulse. The field strengths are $E_{0,\omega} = 2.1$ V/nm and $E_{0,2\omega} = 0.3$ V/nm. The maximal current is observed when both pulses are in temporal overlap. The blue dashed line marks the main overlap region of the laser pulses. The wings, enclosed by the blue dashed line, represent excitation resulting from interference requiring electronic coherence. The gray line considers both the Gaussian distribution and the two error functions accounting for the wings. **b**, Magnification of the central area of (a). A sine function with the frequency of 2ω ($2\pi \cdot 750$ THz) is shown as thick light line. **c**, Fourier transform (FT) amplitude of the data in (a). The current consists almost exclusively of an oscillatory component at 2ω. **d, e** Amplitude of the $\omega + 2\omega$ current as a function of $E_{0,\omega}$ and $E_{0,2\omega}$. **d**, $E_{0,\omega}$ is varied between 1.9 V/nm and 3 V/nm, while $E_{0,2\omega}$ was fixed to 0.07 V/nm. **e**, $E_{0,2\omega}$ takes values between 0.06 V/nm and 0.5 V/nm, with $E_{0,\omega}$ fixed to 2.1 V/nm. The solid lines are linear fits of the double logarithmic representation, indicating the perturbative order of the response: ~ 2 for the variation of $E_{0,\omega}$ and ~ 1 for $E_{0,2\omega}$.

tive phase-dependent current as given by Eq. (1). For further noise suppression, we apply post-processing filters to eliminate high-frequency noise and DC-like contributions, which may occur due to sample imperfections [33].

Figure 2a shows the phase-dependent current as a function of the temporal delay Δt. The applied peak electric field strengths are $E_{0,\omega} = 2.1$ V/nm and $E_{0,2\omega} = 0.3$ V/nm, resulting in a maximal $\omega + 2\omega$ current of 5 nA.

The central region of the overlap scan is magnified in Fig. 2b. Changing the temporal delay Δt by a quarter period of the 2ω field, i.e., by $T_{2\omega}/4 = 0.34\,\text{fs}$, results in a fully symmetric two-color field and no current is measured. Delaying the two pulses by $T_{2\omega}/2 = 0.68\,\text{fs}$ reverses the current direction. The amplitude of the Fourier transform over the entire phase-sensitive current signal, shown in Fig. 2c, exhibits a clear peak at $2\omega = 2\pi \cdot 750\,\text{THz}$ ($800\,\text{nm} \,\hat{=}\, 375\,\text{THz}$), as also expected from Eq. (1). Additionally, we determine the scaling of the current amplitude $|j_{\text{amp.}}|$ as a function of $E_{0,\omega}$ and $E_{0,2\omega}$. We observe a power-law scaling of non-linearities of $\mathcal{N}_\omega = 1.86 \pm 0.15$ and $\mathcal{N}_{2\omega} = 1.09 \pm 0.10$ for the variation of $E_{0,\omega}$ and $E_{0,2\omega}$, respectively (Figs. 2d, 2e), which also supports Eq. (1). Hence, the periodicity of the current modulation as a function of the delay and the power-law scaling corroborate the $\omega + 2\omega$ excitation scheme even in the presence of broadband excitation.

The entire signal shown in Fig. 2a consists of two regimes. The inner part resembles a Gaussian distribution with a width of 17 fs (FWHM, blue dashed line), and an asymmetric outer part with a broadening of the signal up to -32 fs for negative delay (2ω arrives first) and 39 fs for positive delay (ω arrives first). To obtain these numbers, we fit a Gaussian envelope with two error functions to the peaks of the oscillatory signal and so determine the envelope, shown as a gray line. Importantly, the signal outside the main overlap region (blue dashed line) is used in the following to determine the coherence time.

To understand the role of electronic coherence more quantitatively in the current generation process, we model the electron dynamics in graphene using a nearest-neighbor tight-binding model of graphene with minimal coupling of the laser field for the applied laser parameters [5, 34, 35]. The residual conduction band population is obtained by numerically integrating the time-dependent Schrödinger equation (TDSE). In the simulation, we use a carrier-envelope phase of zero for the fundamental to avoid current generation due to the low temporal symmetry of the fundamental pulse [5]. Thus, all currents obtained in the following are of two-color nature.

We discuss the simulation results of the delay-dependent current in two parts: (A), when both pulses do *not* temporally overlap, and (B), when both pulses do temporally overlap. These cases are marked with labels A and B throughout Fig. 3. In Fig. 3a (case A) both pulses are temporally separated by $\Delta t = 35$ fs, and thus hardly overlap in time. Figure 3b shows the corresponding numerically obtained residual conduction band (CB) population ρ_{CB} around the K-point. In the spectral overlap region of the two colors, i.e, at the $2\hbar\omega$ resonance line, ρ_{CB} is determined by the relative phase between the two absorption pathways (illustrated in Fig. 3c with the red and blue arrows). A population imbalance between k-states on the left and right side of the K-points results in a net current. For $\Delta t = 0$, all resonantly excited k-states experience the same spectral phase. Increasing Δt intro-

duces an additional spectral phase $\varphi_{\text{Delay}}(\Delta t, \omega) = 2\omega\Delta t$ and, thus, a spectrally dependent phase at each k-point. As a result, the population distribution becomes modulated as a function of the spectral excitation energy, as shown in the numerical results (see the magnified area in Fig. 3b) and schematically illustrated in Fig. 3c with the filled and solid circles. Depending on the phase the interference at each single k-point is either constructive resulting in excitation or destructive, resulting in no excitation.

Before we discuss this further, we note that in case B, both pulses temporally overlap, as shown in Fig. 3d. Here, electrons experience asymmetric trajectories (intraband motion), resulting in additional symmetry breaking and off-resonant excitation (see Fig. 3a larger errors for $k_x > 0$ and Fig. 3f). As a result, Fig. 3e reveals a strongly asymmetric resonant and off-resonant residual population distribution [24, 36].

To understand how a residual current emerges, we first evaluate ρ_{CB} along constant energies between valence and conduction band $E = E_{\text{CB}} - E_{\text{VB}}$ (see inset of Fig. 3g, example orange rings around the K-point). The current at $E = 3.1\,\text{eV}$ corresponds to the energy of one photon absorption of the 2ω pulse ($1 \times 3.1\,\text{eV}$) and two-photon absorption of the ω pulse ($2 \times 1.55\,\text{eV}$). In Fig. 3g we plot the current as function of energy E for delays ranging from -50 fs to 50 fs. Finally, integration over all energies results in the total residual current (Fig. 3h). This current is maximized when both pulses are in temporal overlap and decreases as a function of delay.

Based on the simulation results we are now able to discuss the role of coherence, coherent dephasing, and off-resonant excitations to the delay-dependent current. When both pulses are temporally separated (case A) we see from Fig. 3g that the two-color current originates from resonant excitation around 3.1 eV. Also in Fig. 3g we see that the spectral phase introduced by the delay results in a shearing of the current modulation in the $E - \Delta t$ plot (see dashed lines). Importantly, it is this shearing that leads to a reduction of the total current after integration (Fig. 3h). This effect is known as coherent dephasing [37], originating from the spectrally dependent phase $\varphi_{\text{Delay}}(\Delta t, \omega)$.

By contrast, when both pulses are in temporal overlap (region B), the current contributions are in phase and do not cancel out each other. Further, additional symmetry-breaking due to the phase-dependent two-color laser field results in off-resonant excitation, which increases the current amplitude. In the method section, we show a video of the temporal evolution of the conduction band population. The video shows most clearly that while in the overlap region B off-resonant excitation emerge. Yet, the main current contribution originates from the resonant excitation, which also matches the observed power-law scalings (Figs. 2d and 2e).

We note that for the applied laser parameters, i.e., $E_{0,\omega} > 1\,\text{V/nm}$ we are in a regime where the Rabi frequency $\Omega_{\text{R}} = v_{\text{F}} e E_0 (\hbar\omega)^{-1}$ becomes comparable to the
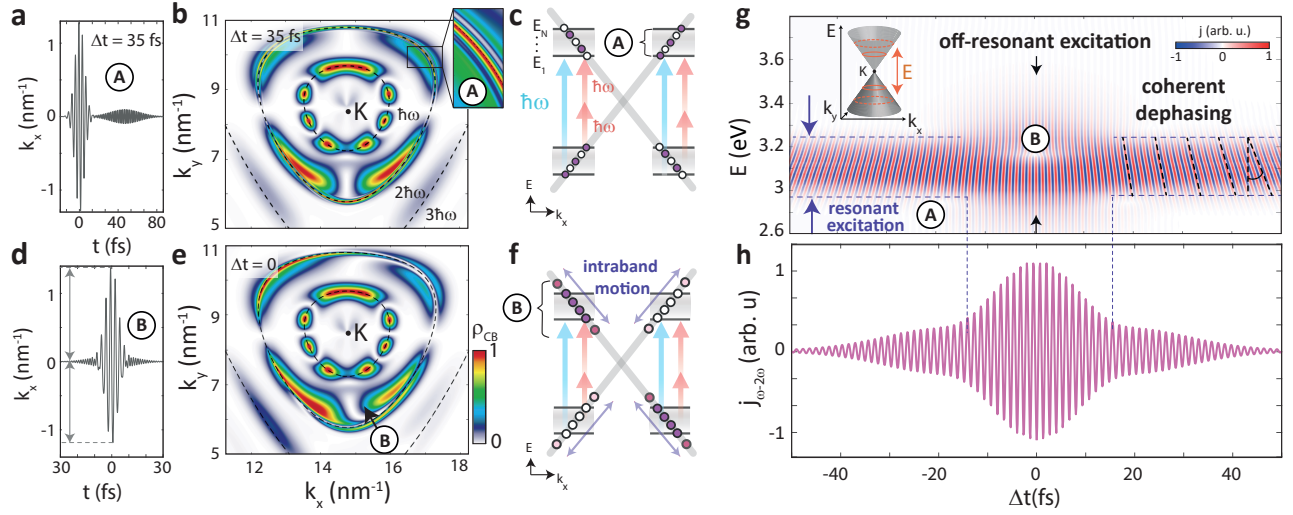
FIG. 3. **Numerical simulation results of two-color excitation in graphene. a,** Electron trajectory $k_x(t)$ for $\Delta t = 35$ fs, when both pulses barely overlap in time. **b,** TDSE results of $\rho_{CB}(k)$ around the K-point after excitation with the two-color laser field ($\Delta t = 35$ fs). $\rho_{CB} = 1$ means that the entire population is transferred from the valence to the conduction band. The dashed lines indicate the resonances, where the energy difference of VB and CB corresponds to the photon energy $\hbar\omega$, $2\hbar\omega$ and $3\hbar\omega$. **c,** Schematic illustration of the current excitation process. Albeit separated in time, one photon absorption with a photon energy of $2\hbar\omega$ and two-photon absorption with a photon energy of $\hbar\omega$ may interfere, governing ρ_{CB}. Due to the broadband optical spectrum of the applied laser fields, several energetic channels contribute to the photocurrent. Each channel accumulates a phase between the pulses given by $2\omega\Delta t$. Averaging over this ensemble of contributions leads to coherent dephasing of the photocurrent. **d-f,** Panels for $\Delta t = 0$. The two arrows in (d) indicate the asymmetry between maximal positive and negative k_x. We note that this asymmetry is almost absent in (a). **g,** Energy-dependent current as a function of Δt. For $|\Delta t| > 17$ fs, excitation is found resonantly only at $2 \times \hbar\omega = \hbar 2\omega$, with a width given by the spectral width of the laser fields. With increasing delay and thus, increasing spectral phase, the population at different excitation energies are more and more out of phase to each other, causing coherent dephasing in the (energy-integrated) residual current (h). When both pulses temporally overlap, additional symmetry breaking results in off-resonant current contributions. **h,** Total current, as a function of Δt.

driving frequency (or photon energy) and a Rabi cycle comparable to the pulse duration [5, 36]. The first gives raise to non-perturbative excitation, as discussed in the previous section in case B. The second, when a Rabi cycle becomes comparable or shorter than the pulse duration or even an optical cycle, coherent depopulation and carrier-wave Rabi flopping may significantly influence the coherent signal. Both processes are naturally included in our TDSE model simulations. For an applied field strength of $E_{0,\omega} = 2.1$ V/nm (as used in Fig. 2a) and an excitation energy of $2\hbar\omega = 3.1$ eV we obtain a Rabi frequency at the peak of the electric field of 677 THz, corresponding to energy of 2.8 eV. So far we have not observed significant deviations from a perturbative power-law scaling, as shown in Fig. 2d, but for higher electric fields strengths and longer laser pulses, we may expect that the coherent control enters the strong-field regime.

The good agreement between experiment (Fig. 2a) and simulation (Fig. 3h) allows us to argue that electronic coherence is preserved at least up to a delay of 32 fs for the negative delay and 39 fs for the positive delay. While the experiment cannot distinguish between coherent dephasing and decoherence caused by scattering, we can only determine a lower bound of the electronic coherence time of 18 fs for the negative delay and 26 fs for a positive delay, given by the error functions (black arrows in

Fig. 2a). Whereas the experiment shows a shorter coherence time when the 2ω pulse arrives first, the simulation shows a symmetric $\omega + 2\omega$ trace. One reason for this asymmetric behavior might be that for $\Delta t < 0$ the first pulse (2ω) generates the population via one-photon absorption, which could lead to a higher total initial population. While the current amplitude, which is the result of interference, is only sensitive to the overlap of the two populations, a possible initial population-dependent decoherence time might break the symmetry [1]. Further simulations accounting for the critical role of decoherence and scattering are required, which are beyond the scope of this work. To determine the decoherence time, we take the mean of both values and obtain 22 ± 4 fs.

By comparing this decoherence time with a reported thermalization time of $50 - 80$ fs, which involves multiple-scattering events, we find that the decoherence time is about 2-3 times shorter [38–40]. Similarly, Auger processes and carrier multiplication can occur on a similar time scale [41, 42]. Subsequent electron cooling and phonon scattering are incoherent processes that occur on a time scale of 100 fs to ps [43, 44] and thus are unlikely to be responsible for the loss of electron coherence.

The coherence time obtained from the photocurrent measurements reflects electronic coherence and coherent dephasing. While the latter reduces the current ampli-

tude, it does not affect the electronic coherence. In coherent spectroscopy, such as in pulse echo experiments, these two dephasing channels are usually considered as T_2^*, reflecting both natural T_2-dephasing and dephasing caused by inhomogeneities in the ensemble [37, 45–48]. By introducing a frequency gradient to one of the pulses, T_2^* can be corrected for coherent dephasing. A similar approach might be possible here, namely by shaping the spectral phase of one of the laser pulses to correct for coherent dephasing. In such a scenario, the observed phase shift of the current as a function of energy, shown in Fig.3g, can be nulled. Then, the photocurrent can directly be used to monitor electronic coherence [37].

In summary, we present a lower boundary for the electronic coherence time in graphene of 22 ± 4 fs. To observe it, we use quantum-path interference and the resulting current, generated by a two-color laser field as an observable. The ultrafast nature of the laser pulses employed and the ability to time delay them offer an ideal probe for monitoring this coherence. By shaping the spectral phase of the laser pulses we propose the possibility to disentangle decoherence and coherent dephasing in a similar manner as applied for pulse echo experiments. We expect this versatile and efficient method for measuring electronic coherence based on a purely electronic observable to find widespread use in vastly different systems and experimental configurations.

[1] J. Y. Bigot, M. T. Portella, R. W. Schoenlein, J. E. Cunningham, and C. V. Shank, "Two-dimensional carrier-carrier screening in a quantum well," Physical Review Letters **67**, 636–639 (1991).

[2] Ferenc Krausz and Mark I. Stockman, "Attosecond metrology: from electron capture to future signal processing," Nature Photonics **8**, 205–213 (2014).

[3] M. Hohenleutner, F. Langer, O. Schubert, M. Knorr, U. Huttner, S. W. Koch, M. Kira, and R. Huber, "Real-time observation of interfering crystal electrons in high-harmonic generation," Nature **523**, 572–575 (2015).

[4] Steven T. Cundiff, "Coherent spectroscopy of semiconductors," Optics InfoBase Conference Papers **16**, 4639–4664 (2016).

[5] Takuya Higuchi, Christian Heide, Konrad Ullmann, Heiko B. Weber, and Peter Hommelhoff, "Light-field-driven currents in graphene," Nature **550**, 224–228 (2017).

[6] Marcel Reutzel, Andi Li, and Hrvoje Petek, "Coherent Two-Dimensional Multiphoton Photoelectron Spectroscopy of Metal Surfaces," Physical Review X **9**, 011044 (2019).

[7] P. Maunz, D. L. Moehring, S. Olmschenk, K. C. Younge, D. N. Matsukevich, and C. Monroe, "Quantum interference of photon pairs from two remote trapped atomic ions," Nature Physics **3**, 538–541 (2007).

[8] Christiane P. Koch and Moshe Shapiro, "Coherent Control of Ultracold Photoassociation," Chemical Reviews **112** (2012).

[9] H. Petek and S. Ogawa, "Femtosecond time-resolved two-photon photoemission studies of electron dynamics in metals," Progress in Surface Science **56**, 239–310 (1997).

[10] L. Seiffert, Q. Liu, S. Zherebtsov, A. Trabattoni, P. Rupp, M. C. Castrovilli, M. Galli, F. Süßmann, K. Wintersperger, J. Stierle, G. Sansone, L. Poletto, F. Frassetto, I. Halfpap, V. Mondes, C. Graf, E. Rühl, F. Krausz, M. Nisoli, T. Fennel, F. Calegari, and M. F. Kling, "Attosecond chronoscopy of electron scattering in dielectric nanoparticles," Nature Physics **13**, 766–770 (2017).

[11] Marcel Reutzel, Andi Li, Zehua Wang, and Hrvoje Petek, "Coherent multidimensional photoelectron spectroscopy of ultrafast quasiparticle dressing by light," Nature Communications **11**, 1–5 (2020).

[12] S. T. Cundiff, "Effects of correlation between inhomogeneously broadened transitions on quantum beats in transient four-wave mixing," Physical Review A **49**, 3114–3118 (1994).

[13] R Atanasov, A Haché, J L P Hughes, H M Van Driel, and J E Sipe, "Coherent Control of Photocurrent Generation in Bulk Semiconductors," Physical Review Letters **76**, 1703–1706 (1996).

[14] A. Haché, Y. Kostoulas, R. Atanasov, J. L.P. Hughes, J. E. Sipe, and Max Glasbeek, "Observation of coherently controlled photocurrent in unbiased, bulk GaAs," Physical Review Letters **78**, 306–309 (1997).

[15] E. Dupont, P. B. Corkum, H. C. Liu, M. Buchanan, and Z. R. Wasilewski, "Phase-controlled currents in semiconductors," Physical Review Letters **74**, 3596–3599 (1995).

[16] T. M. Fortier, P. A. Roos, D. J. Jones, S. T. Cundiff, R. D. R Bhat, and J. E. Sipe, "Carrier-envelope phase-controlled quantum interference of injected photocurrents in semiconductors," Physical Review Letters **92**, 147403 (2004).

[17] Dong Sun, Charles Divin, Julien Rioux, John E. Sipe, Claire Berger, Walt A. De Heer, Phillip N. First, and Theodore B. Norris, "Coherent control of ballistic photocurrents in multilayer epitaxial graphene using quantum interference," Nano Letters **10**, 1293–1296 (2010).

[18] Dong Sun, Charles Divin, Momchil Mihnev, Torben Winzer, Ermin Malic, Andreas Knorr, John E Sipe, Claire Berger, Walt A de Heer, Phillip N First, and Theodore B Norris, "Current relaxation due to hot car-

rier scattering in graphene," New Journal of Physics **14**, 105012 (2012).

[19] J. A. Armstrong, N. Bloembergen, J. Ducuing, and P. S. Pershan, "Interactions between light waves in a nonlinear dielectric," Physical Review **127**, 1918–1939 (1962).

[20] Antonio J. Garzón-Ramírez and Ignacio Franco, "Stark control of electrons across interfaces," Physical Review B **98**, 121305(R) (2018).

[21] Antonio J Grzón-Ramírez and Ignacio Franco, "Symmetry breaking in the Stark Control of Electrons at Interfaces (SCELI)," The Journal of Chemical Physics **153**, 044704 (2020).

[22] Valérie Blanchet, Céline Nicole, Mohamed Aziz Bouchene, and Bertrand Girard, "Temporal coherent control in two-photon transitions: From optical interferences to quantum interferences," Physical Review Letters **78**, 2716–2719 (1997).

[23] Ignacio Franco and Paul Brumer, "Minimum requirements for laser-induced symmetry breaking in quantum and classical mechanics," Journal of Physics B: Atomic, Molecular and Optical Physics **41**, 074003 (2008).

[24] Michael S. Wismer, Stanislav Yu Kruchinin, Marcelo Ciappina, Mark I. Stockman, and Vladislav S. Yakovlev, "Strong-Field Resonant Dynamics in Semiconductors," Physical Review Letters **116**, 197401 (2016).

[25] Larisa A Chizhova, Florian Libisch, and Joachim Burgdörfer, "Nonlinear response of graphene to a few-cycle terahertz laser pulse: Role of doping and disorder," Physical Review B **94**, 075412 (2016).

[26] Shunsuke A. Sato, Matteo Lucchini, Mikhail Volkov, Fabian Schlaepfer, Lukas Gallmann, Ursula Keller, and Angel Rubio, "Role of intraband transitions in photocarrier generation," Physical Review B **98**, 035202 (2018).

[27] Moshe Shapiro and Brumer Paul, Quantum control of molecular processes (John Wiley & Sons, 2012).

[28] Bing Gu and Ignacio Franco, "Quantifying Early Time Quantum Decoherence Dynamics through Fluctuations," Journal of Physical Chemistry Letters **8**, 4289–4294 (2017).

[29] Wenxiang Hu, Bing Gu, and Ignacio Franco, "Lessons on electronic decoherence in molecules from exact modeling," Journal of Chemical Physics **148**, 1–11 (2018).

[30] Elsa Cassette, Ryan D. Pensack, Benoît Mahler, and Gregory D. Scholes, "Room-temperature exciton coherence and dephasing in two-dimensional nanostructures," Nature Communications **6**, 6086 (2015).

[31] Peter M. Kraus, Michael Zürch, Scott K. Cushing, Daniel M. Neumark, and Stephen R. Leone, "The ultrafast X-ray spectroscopic revolution in chemical dynamics," Nature Reviews Chemistry **2**, 82–94 (2018).

[32] Romain Geneaux, Hugo J.B. Marroux, Alexander Guggenmos, Daniel M. Neumark, and Stephen R. Leone, "Transient absorption spectroscopy using high harmonic generation: A review of ultrafast X-ray dynamics in molecules and solids," Philosophical Transactions of the Royal Society A: Mathematical, Physical and Engineering Sciences **377**, 2145 (2019).

[33] Erin Sheridan, Lu Chen, Jianan Li, Qing Guo, Shan Hao, Muqing Yu, Ki Tae Eom, Hyungwoo Lee, Jung Woo Lee, Chang Beom Eom, Patrick Irvin, and Jeremy Levy, "Gate-Tunable Optical Nonlinearities and Extinction in Graphene/LaAlO3/SrTiO3Nanostructures," Nano Letters **20**, 6966–6973 (2020).

[34] Hamed Koochaki Kelardeh, Vadym Apalkov, and Mark I. Stockman, "Graphene in ultrafast and superstrong laser fields," Physical Review B **91**, 045439 (2015).

[35] Q. Z. Li, P. Elliott, J. K. Dewhurst, S. Sharma, and S. Shallcross, "Ab initio study of ultrafast charge dynamics in graphene," Physical Review B **103**, L081102 (2021).

[36] Chrisitan Heide, Tobias Boolakee, Takuya Higuchi, and Peter Hommelhoff, "Adiabaticity parameters for the categorization of light-matter interaction – from weak to strong driving," (2021), arXiv:2104.10112.

[37] Serge Haroche and J-M. Raimond, Exploring the Quantum: Atoms, Cavities, and Photons (Oxford University Press, Oxford, 2006) pp. 0–3.

[38] M. Breusing, S. Kuehn, T. Winzer, E. Malić, F. Milde, N. Severin, J. P. Rabe, C. Ropers, A. Knorr, and T. Elsaesser, "Ultrafast nonequilibrium carrier dynamics in a single graphene layer," Physical Review B - Condensed Matter and Materials Physics **83**, 153410 (2011).

[39] K. J. Tielrooij, L. Piatkowski, M. Massicotte, A. Woessner, Q. Ma, Y. Lee, K. S. Myhro, C. N. Lau, P. Jarillo-Herrero, N. F. Van Hulst, and F. H.L. Koppens, "Generation of photovoltage in graphene on a femtosecond timescale through efficient carrier heating," Nature Nanotechnology **10**, 437–443 (2015).

[40] Isabella Gierz, Jesse C. Petersen, Matteo Mitrano, Cephise Cacho, I. C.Edmond Turcu, Emma Springate, Alexander Stöhr, Axel Köhler, Ulrich Starke, and Andrea Cavalleri, "Snapshots of non-equilibrium Dirac carrier distributions in graphene," Nature Materials **12**, 1119–1124 (2013).

[41] Torben Winzer, Andreas Knorr, and Ermin Malic, "Carrier multiplication in graphene," Nano Letters **10**, 4839–4843 (2010).

[42] D. Brida, A. Tomadin, C. Manzoni, Y. J. Kim, A. Lombardo, S. Milana, R. R. Nair, K. S. Novoselov, A. C. Ferrari, G. Cerullo, and M. Polini, "Ultrafast collinear scattering and carrier multiplication in graphene," Nature Communications **4**, 1–9 (2013), arXiv:1209.5729.

[43] Matt W. Graham, Su Fei Shi, Daniel C. Ralph, Jiwoong Park, and Paul L. McEuen, "Photocurrent measurements of supercollision cooling in graphene," Nature Physics **9**, 103–108 (2013), arXiv:1207.1249.

[44] Søren Ulstrup, Jens Christian Johannsen, Alberto Crepaldi, Federico Cilento, Michele Zacchigna, Cephise Cacho, Richard T Chapman, Emma Springate, Felix Fromm, Christian Raidel, Thomas Seyller, Fulvio Parmigiani, Marco Grioni, and Philip Hofmann, "Ultrafast electron dynamics in epitaxial graphene investigated with time- and angle-resolved photoemission spectroscopy," Journal of Physics: Condensed Matter **27**, 164206 (2015).

[45] E. L. Hahn, "Spin echoes," Physical Review **80**, 580–594 (1950).

[46] N. A. Kurnit, I. D. Abella, and S. R. Hartmann, "Observation of a photon echo," Physical Review Letters **13**, 567–568 (1964).

[47] Ady Stern, Yakir Aharonov, and Yoseph Imry, "Phase uncertainty and loss of interference: A general picture," Physical Review A **41**, 3436–3448 (1990).

[48] Koichi Oshio and David A. Feinberg, Magnetic Resonance in Medicine, Tech. Rep. 344-349 (1991).